# Pulse profile stability of the Crab pulsar

Chetana Jain[1] and Biswajit Paul[2]

[1]  Hans Raj College, University of Delhi, Delhi-110007, India; *chetanajain11@gmail.com*
[2]  Raman Research Institute, Sadashivnagar, C. V. Raman Avenue, Bangalore 560080, India

**Abstract**  We present an X-ray timing analysis of the Crab pulsar, PSR B0531+21, using archival *RXTE* data. We have investigated the stability of the Crab pulse profile, in soft ($2-20$ keV) and hard ($30-100$ keV) X-ray energies, over the last decade of *RXTE* operation. The analysis includes measurement of the separation between the two pulse peaks and the intensity and widths of the two peaks. We did not find any significant time dependency in the pulse shape. The two peaks have been stable in phase, intensity and width for the last ten years. The first pulse is relatively stronger at soft X-rays. The first pulse peak is narrower than the second peak in both soft and hard X-ray energies. Both the peaks show a slow rise and a steeper fall. The ratio of the pulsed photons in the two peaks is also constant in time.

**Key words:** pulsars: individual: Crab (PSR B0531+21) — stars: neutron — X-rays

## 1 INTRODUCTION

The Crab pulsar (PSR B0532+21) was discovered in 1968 (Staelin & Reifenstein 1968) and is the remnant of a supernova explosion (SN 1054). The neutron star rotates about 30 times per second. The pulsed emission is visible across the entire electromagnetic spectrum (radio: Hankins & Eilek 2007, optical: Oosterbroek et al. 2008, X-rays: Mineo et al. 2006, $\gamma$-rays: Kuiper et al. 2001 and very high energy: Aliu et al. 2008).

In all energy bands, the Crab pulsar's pulse profile exhibits a dual peak structure and the pulse morphology is known to vary as a function of photon energy. The two peaks are separated by a phase of $\sim 0.4$ over all the wavelengths (Pravdo et al. 1997; Kuiper et al. 2003; Rots et al. 2004). However, the arrival times of the two peaks are not aligned in phase at different wavelengths. X-ray and $\gamma$-ray pulses lead the radio pulse (Kuiper et al. 2003; Rots et al. 2004; Abdo et al. 2010). The phase delay measurements between optical and radio observations show a fuzzy behavior, with reports of the optical pulse leading (Oosterbroek et al. 2006), trailing behind (Golden et al. 2000) and being coincident with (Romani et al. 2001) the radio pulse.

The variation of the Crab pulsar's pulse profile as a function of photon energy has been studied many times in significant detail. The relative intensities of the two pulse peaks move in a see-saw manner with increasing energy. The first peak is more pronounced at radio and optical wavelengths (Oosterbroek et al. 2008). The second peak starts to dominate as energy increases and eventually towers above the former at soft $\gamma$-rays (Mineo et al. 2006). With a further increase in energy, the first peak again becomes dominant (Kuiper et al. 2001).

The time variability of the Crab pulsar pulse profile is relatively less studied (Jones et al. 1980; Carraminana et al. 1994). Nevertheless, it is equally important. It can assist our understanding of the emission nature of this object. Irrespective of the physical internal process in the neutron star, phenomena that can possibly change the high energy pulse profile of a rotation powered pulsar are: (i) some reconfiguration of the neutron star crust and magnetic field structure, which can be associated with starquaks and glitches (Franco et al. 2000) and (ii) changes in the neutron star spin axis with respect to the line of sight, which can happen due to precession (Melatos 2000). Some variations of the gamma-ray pulse profile of the Crab pulsar were interpreted to be due to a 13-year precession (Nolan et al. 1993; Ulmer et al. 1994). Pulsar glitches are expected to produce thermal X-rays (Hui & Cheng 2004) and a certain form of energy release can also produce pulsed X-ray emission (Tang & Cheng 2001; Cheng et al. 1998), which can change the pulse profiles for some period after the glitches.

In this paper, we present the first ever long-term pulse shape analysis of the Crab pulsar, using data spread over ten years (2001–2010). Observations made with the instruments onboard the *RXTE* satellite were used to analyze the evolution of the pulse profile in soft ($2-20$ keV) and hard ($30-100$ keV) X-ray energy bands. In Section 2, we describe the data reduction from the *RXTE*-PCA and HEXTE instruments. This section also explains the model used to quantify the observations. The results obtained from the detailed timing analysis are discussed in Section 3. We summarize and discuss the implications of the observations in Section 4.

## 2 OBSERVATIONS AND ANALYSIS

Data for the present analysis were obtained from two different detectors onboard the *RXTE*: (i) the Proportional Counter Array (PCA) and (ii) the High-Energy X-ray Timing Experiment (HEXTE). The field of view of these non-imaging detectors contained both the Crab pulsar and the Crab nebula. The data used in the present analysis are in the 2–20 keV band from the PCA detectors and in the 30-100 keV band from the HEXTE instrument. The Crab nebula suffered significant scattering during 1995–1998 (Wong et al. 2001; Rots et al. 2004). Therefore, we did not include data before this period, so as to avoid misleading results due to the broadening of the pulses. The entire analysis was done using the FTOOL from the astronomy software HEASOFT-ver 5.2. The following subsections give the details of PCA and HEXTE data reduction.

### 2.1 Reduction of *RXTE*-PCA Data

The *RXTE*-PCA consists of an array of five collimated xenon/methane multi-anode proportional counter units (PCU) with a total photon collection area of 6500 cm$^2$ (Jahoda et al. 1996, 2006). Data are available in different event modes and they are binned into different energy channels. For the present work, we have used all the publicly available data in event mode E_250$\mu$s_128M_0_1s. This data mode has a time resolution of 250 $\mu$s and energy information is spread over 128 channels. Selection of this mode allowed us to obtain uniformity over the energy bins during a long timebase from 2001–2010.

From each observation, energy resolved pulse folded light curves were generated using the FTOOL-FASEBIN. This tool corrects the photon arrival times and converts them to the solar system barycenter. The arrival time of each event is then converted into the phase of the rotational period of the pulsar. The output of FASEBIN is a two dimensional histogram of photon count rate against the pulse phase and energy. Absolute phase was determined by using the time solution available from the Jodrell Bank Crab Pulsar Monthly Ephemeris[1] (Lyne et al. 1993) and the corresponding pulsar coordinates. Thereafter, another FTOOL - FBSSUM was used, which integrates the pulse profiles over different energy ranges.

---

[1] *http://www.jb.man.ac.uk/*
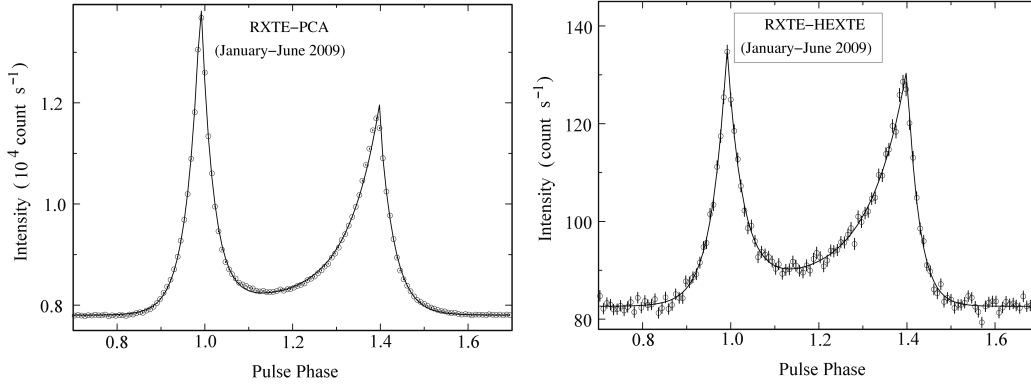
**Fig. 1** A sample of $2-20$ keV and $30-100$ keV pulse profiles of the Crab pulsar from *RXTE*-PCA and HEXTE observations. The solid line shows the best fit model, with a reduced $\chi^2$ of 1.3 and 0.9, for 118 d.o.f., respectively. The observation details are mentioned in each panel.

A typical $2-20$ keV *RXTE*-PCA pulse profile, binned into 128 phasebins, is shown in Figure 1 (left panel). The figure shows the average profile of all the observations made between January to June, 2009. The average profile was generated using the FTOOL-FBADD. The folded light curve has an asymmetric, dual-peak shape. The first pulse is stronger than the second pulse. A significant inter-peak emission (bridge emission) is also seen. Hereafter, the first peak will be referred to as "P1" and the second peak as "P2."

## 2.2 Reduction of *RXTE*-HEXTE Data

The *RXTE*-HEXTE consists of two clusters, each containing four NaI/CsI phoswich scintillation detectors, with a total photon collection area of $1600 \text{ cm}^2$ (Rothschild et al. 1998). Each of these clusters rock along mutually orthogonal directions to provide background measurements. When cluster-0 is on target, cluster-1 is off target and vice-versa, i.e. the HEXTE rocks between on- and off- source positions. For the present work, data in science event mode were analyzed from all the observations made between 2001–2010. From the raw science event files, the source files were generated, using the FTOOL-HXTBACK. Energy resolved pulse profiles were obtained using the FTOOLS- FASEBIN and FBSSUM. The FASEBIN extracts only the on-source data from the raw file. The HEXTE data were also folded with the same radio ephemeris, as in the case of PCA data.

Figure 1 (right panel) shows a sample of the average $30-100$ keV pulse profile of the Crab pulsar from data obtained between January–June, 2009. As opposed to the soft X-ray pulse profile, the data above 30 keV have low statistics. We have therefore, separately generated HEXTE pulse profiles by averaging the data on a half yearly basis.

## 2.3 Model Fitting

To quantify the analysis, we fitted a 10-parameter model to the pulse profiles. The model consisted of: the position and peak intensity of each pulse peak; two exponentials (one rise and one decay) for each pulse peak; and two constants (one for the nebular and background emission, and the other for the inter-peak emission). The model was fitted over the phase range 0.7–1.7. An example of the best fit model is shown with a solid line, in Figure 1, for the PCA and HEXTE profiles. The reduced $\chi^2$ of the best fit ranged between 0.6 and 3.5, for 118 degrees of freedom.

## 3 RESULTS

All the pulse profiles of *RXTE*-PCA and HEXTE were fitted with the model as described above. The variability/stability of the important parameters of the fit are discussed below. Several glitches have been detected from the Crab pulsar in the period of these X-ray data. The times at which the glitches occurred (taken from Espinoza et al. (2011)) are marked in the top panel of each subsequent figure. All glitches, except for one, had similar magnitudes ($\Delta\nu/\nu$ of $\sim 10 \times 10^{-9}$), while one of them (which occurred around MJD 53067) had a magnitude of $\sim 200 \times 10^{-9}$.

### 3.1 Separation of the Two Pulse Peaks

As shown in the sample pulse profiles in Figure 1, two clear peaks are seen at phases $\sim$0.99 and $\sim$1.39. Figure 2 shows the separation between the two peaks, from the *RXTE*-PCA and HEXTE observations. The X-axis in this figure gives the MJD of the respective observation and the Y axis gives the phase separation between the two peaks.
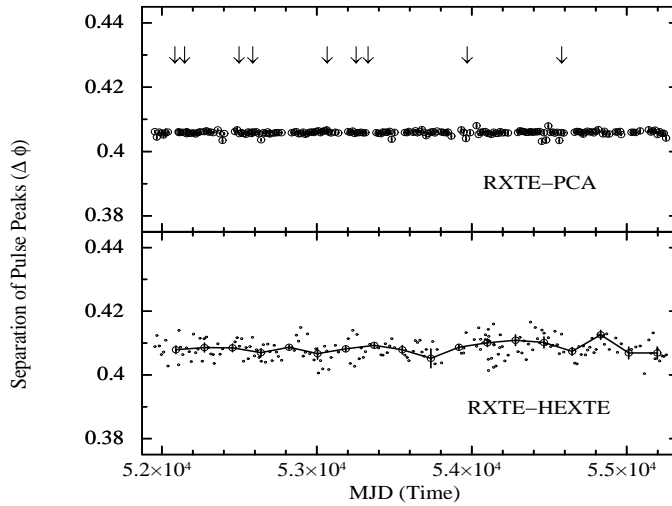


**Fig. 2** The separation between the two pulse peaks of the Crab pulse profile, from *RXTE*-PCA and HEXTE observations. The solid line in the bottom panel shows the half-yearly trend in HEXTE. Arrows in the top panel indicate the time of occurrence of glitches.

A constant fit to the *RXTE*-PCA curve gave a phase separation of 0.4058 (5), with a reduced $\chi^2$ of 0.94 for 189 d.o.f. A constant fit to the HEXTE results gave a phase separation of 0.4079 (6) between the two pulse peaks. The reduced $\chi^2$ of the fit was 0.36 for 188 d.o.f. The solid line in the results from the HEXTE detector shows the half yearly trend. This indicates that the pulse peak maxima are stable in time. The separation of the maxima of the two peaks is constant over the last ten years. Furthermore, the phase separation between the two peaks does not show a significant variation with energy, consistent with earlier observations (Wills et al. 1982; Clear et al. 1987; Nolan et al. 1993). We did not find any considerable effect of the occurrence of glitches on the separation between the pulse peak maxima.

## 3.2 Pulse Widths

The rise and decay times of P1 and P2 (in phase units), for the PCA and HEXTE pulse profiles, are shown in Figure 3, along with the occurrence of glitches in the top panel. The X-axis gives the MJD of each observation. In the case of HEXTE, the half yearly average trend is shown with a solid line. A constant was fit and results are given in Table 1, with the 90% confidence limit and $\chi^2$ of fitting. The reduced $\chi^2$ is $\sim 1$ for all the parameters, except for the decay time of the first peak. This could be due to a small variation in the arrival time of the main pulse, as has been reported earlier using the Egret data, and needs to be studied in detail for the *RXTE* data (Kuiper et al. 2003). In both of the energy bands, the two pulses are asymmetric. Both peaks, P1 and P2, show a slower rise and a steep fall. The first pulse peak is narrower than the second peak. It rises in almost half the time taken by the second peak. The first peak also decays faster than the second peak. We did not find any detectable effect of occurrence of glitches on the pulse widths.
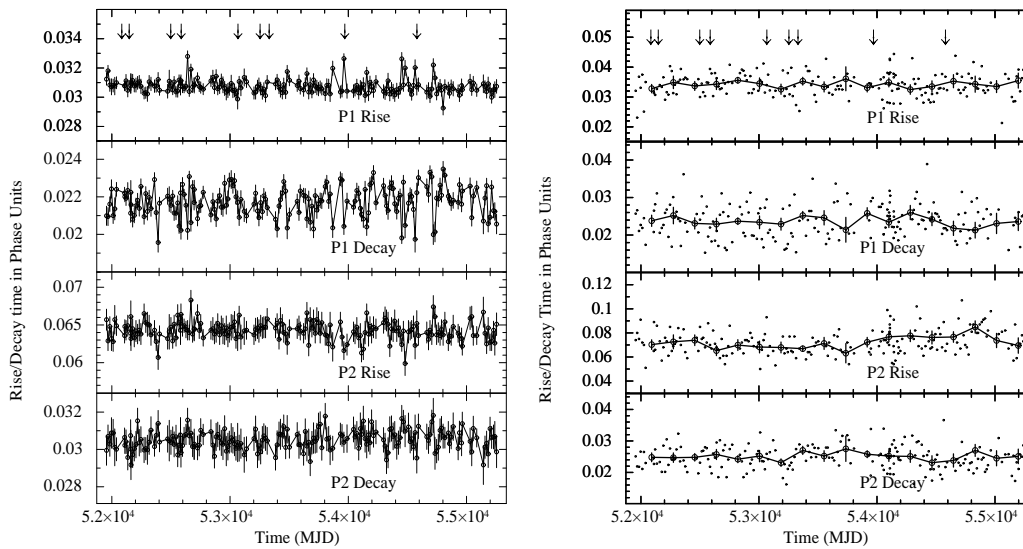


**Fig. 3** The rise and decay times of the two peaks of the Crab pulse profile. The left panels show the results from *RXTE*-PCA observations, while the HEXTE results are shown in the right panels. The half yearly trend of the HEXTE observations is shown with a solid line in the figure. The arrows indicate the occurrence time of the glitches.

## 3.3 Pulsed Intensity

Figure 4 shows the ratio of the integrated pulsed photons in the two peaks for *RXTE*-PCA and HEXTE observations. A constant fit to the two ratios gave a value of 0.633 (1) for the PCA and 0.604 (13) for the HEXTE energy bands. This result is consistent with results reported using *COMPTEL* observations at medium $\gamma$-ray energies (1–10 MeV) (Buccheri et al. 1993; Carraminana et al. 1994; Kuiper et al. 2001) and from *EGRET* observations above 30 MeV (Fierro 1995; Tompkins et al. 1997). However, more variation is seen in the HEXTE data as compared to the PCA results, which might be due to poorer statistics in the case of the HEXTE data. Furthermore, although the second peak is smaller, it contains a large number of pulsed photons.

**Table 1** Results for model fitting of the Crab pulse profile.

| Parameter | *RXTE*-PCA | | *RXTE*-HEXTE | |
|---|---|---|---|---|
| | Value | Reduced $\chi^2$ (for 189 d.o.f.) | Value | Reduced $\chi^2$ (for 188 d.o.f.) |
| Phase separation between the two pulse peaks | 0.4058 (5) | 0.94 | 0.4079 (6) | 0.36 |
| Rise time of P1 (in phase unit) | 0.03077 (5) | 1.3 | 0.0335 (6) | 0.43 |
| Decay time of P1 (in phase unit) | 0.02180 (4) | 3.5 | 0.0236 (12) | 2.5 |
| Rise time of P2 (in phase unit) | 0.0642 (1) | 0.75 | 0.0707 (15) | 0.44 |
| Decay time of P2 (in phase unit) | 0.03051 (8) | 0.52 | 0.0241 (5) | 0.49 |
| Ratio of pulsed photons in the two peaks (P1/P2) | 0.633 (1) | 0.63 | 0.604 (13) | 0.39 |
| Pulse intensity ratio (P1/P2) | 1.6344 (35) | 0.8 | 1.18 (2) | 0.33 |

∗ The numbers in brackets give the error for a 90% confidence range in the respective values.
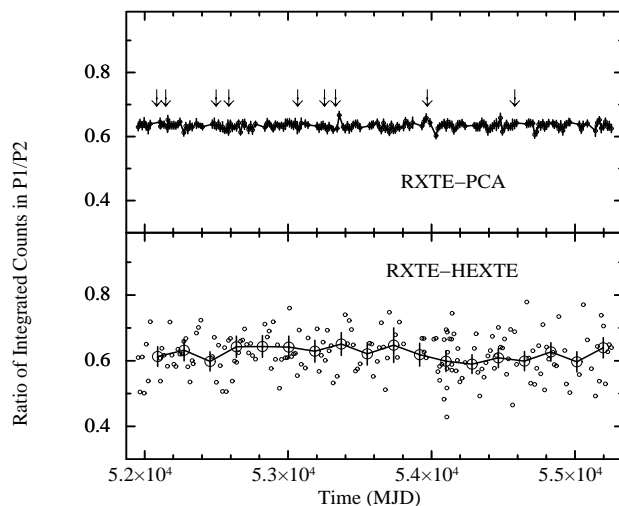


**Fig. 4** The ratio of integrated counts in P1 to P2, for *RXTE*-PCA and HEXTE observations, as a function of time. The arrows indicate the occurrence times of the glitches.

### 3.4 Pulse Intensity Ratio

A comparison of the variation in the intensity ratio of the amplitude of the two pulse peaks in the PCA and HEXTE profiles is shown in Figure 5. Here, the intensity ratio of the two peaks (P1/P2) is plotted as a function of time. A ratio of 1 or above indicates that the first peak is dominant, whereas a ratio of less than 1 implies a stronger second peak. Clearly, P1 is significantly stronger than P2 in the soft X-ray band (PCA data). A constant fit gave an intensity ratio of 1.63, with a reduced $\chi^2$ of 0.8 for 189 d.o.f. The intensity ratio of the HEXTE pulses shows a variation, which could be due to poorer statistics. The solid line in the figure shows the half yearly average trend in the intensity ratio of HEXTE profiles. A constant fit in the case of the HEXTE results gave an intensity ratio of 1.18, with a reduced $\chi^2$ of 0.33 for 188 d.o.f. Clearly, the first peak also dominates at higher energy, albeit the ratio is smaller.

### 4 DISCUSSION

A coherent picture of the pulsed emission from the Crab pulsar has been an enigma, despite numerous multi-wavelength studies. The radiation in radio, optical, X-rays and high energy $\gamma$-rays is
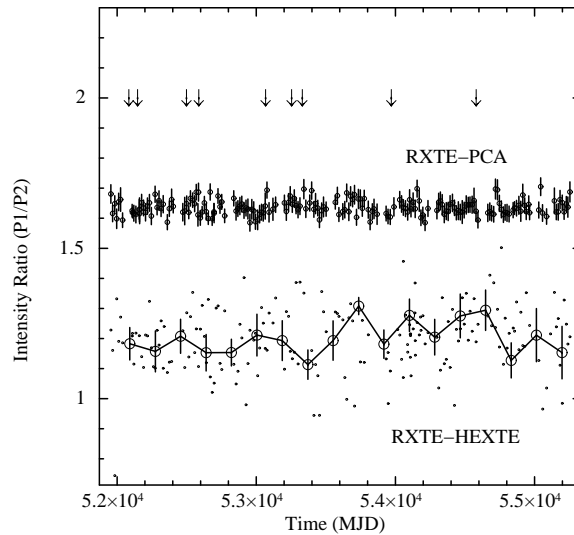
**Fig. 5** The variation of intensity ratios of the two pulse peaks (P1/P2) of the Crab pulsar is shown as a function of time. The curve at the top shows the variation for PCA observations, while the curve below corresponds to HEXTE observations. The solid line in the lower curve shows the half yearly average trend in the HEXTE observations. The arrows indicate the occurrence time of the glitches.

known to differ considerably. In this paper, we have reported that the X-ray pulse profile of the Crab pulsar has been stable in time over the last ten years of *RXTE* performance. There has been no indication of time variability of the pulse shape at soft and hard X-ray energies during the last decade of observations. No evidence of time variation has been noticed in the phase separation between the two pulse peaks, the widths of the two peaks or their relative intensities.

The light curves of X-ray pulsars reflect the geometry of the magnetic field and the radiation emission pattern of the rotating object. If the pulses are produced near the neutron star surface, the compactness (mass-to-radius ratio) of the neutron star will also cause gravitational bending of light and thus affects the pulse profile. There are several reports on the long-term flux variability of the Crab pulsar. This is conjectured to be due to the slow precession of the spin axis of the neutron star, which results in precession of the pulsar's magnetosphere at similar periods (Özel 1989; Kanbach 1990; Nolan et al. 1993; Ulmer et al. 1994). Since the X-ray and $\gamma$-ray emission is modulated by the magnetosphere geometry, changes in the respective pulse profiles should be synchronized. Flux variability can also be attributed to sudden glitch-induced changes between the pulsar spin axis and the magnetic moment axis (Link et al. 1992; Link & Epstein 1997; Franco et al. 2000). A change in the alignment angle during a glitch can modulate the duration of the line of sight's traverse through the pulse emission cone. This in turn can produce considerable differences in the pulsed emission from the neutron star (Jones et al. 1980; Sekimoto et al. 1995).

However, if these theories are true, then the pulsed X-ray and the $\gamma$-ray emissions are supposed to show similar variations. The $\gamma$-ray pulse profile of the Crab pulsar shows considerable variations over time. The intensity ratio of the two peaks in the pulsar's light curve is known to undergo a periodic behavior (Wills et al. 1982; Özel 1991; Nolan et al. 1993; Ulmer et al. 1994) at high $\gamma$-ray energies. However, we have found that the intensity ratio of the two peaks is stable in time, both in soft and hard X-rays. This is consistent with earlier works in the X-ray band (Wills et al. 1982). It has been proposed that the periodic variability in the intensity ratio of the two peaks is masked at lower photon energies due to the onset of plasma-dominated radiation, which mainly affects the second

pulse peak (Hasinger et al. 1984; Hasinger 1985). However, neither the magnitude of the radiation component is certain, nor are there supportive conclusions from the optical and radio observations.

The emission of thermal radiation from the neutron star is also affected by the turmoil in its interior. It could be due to the rotational dynamics of the superfluid in the neutron star's inner crust. The X-ray light curve can also become modulated due to the release of a large amount of X-ray energy during the sudden onset of glitches (Hui & Cheng 2004). However, we have seen that the pulse profile is constant in time. There are no significant changes in the pulse shape parameters during glitches. Therefore, it is difficult to comment on the extent of turbulence caused by them.

The underlying physics involved in the emission mechanism of the Crab pulsar is not completely understood and a coordinated multi-waveband study of the pulsar is crucial. Our results fill in the gaps between the trend seen at other wavelengths and we hope that observations by more sensitive instruments on future missions, like $ASTROSAT$ (Paul & The LAXPC Team 2009), will provide important clues regarding the pulsar emission mechanism.

# References

Abdo, A. A., Ackermann, M., Ajello, M., et al. 2010, ApJ, 708, 1254

Aliu, E., Anderhub, H., Antonelli, L. A., et al. 2008, Science, 322, 1221

Buccheri, R., Bennett, K., Busetta, M., et al. 1993, Advances in Space Research, 13, 727

Carraminana, A., Bennett, K., Buccheri, R., et al. 1994, A&A, 290, 487

Cheng, K. S., Li, Y., & Suen, W. M. 1998, ApJ, 499, L45

Clear, J., Bennett, K., Buccheri, R., et al. 1987, A&A, 174, 85

Espinoza, C. M., Lyne, A. G., Stappers, B. W., & Kramer, M. 2011, MNRAS, 414, 1679

Fierro, J. M. 1995, Observ. of Spin-Powered pulsars with EGRET, Ph.D. Thesis, Stanford University

Franco, L. M., Link, B., & Epstein, R. I. 2000, ApJ, 543, 987

Golden, A., Shearer, A., Redfern, R. M., et al. 2000, A&A, 363, 617

Hankins, T. H., & Eilek, J. A. 2007, ApJ, 670, 693

Hasinger, G. 1985, in The Crab Nebula and Related Supernova Remnants, Proceedings of the Workshop, eds. M. C. Kafatos, & R. B. C. Henry (Cambridge: Cambridge University Press), 47

Hasinger, G., Pietsch, W., Reppin, C., et al. 1984, Advances in Space Research, 3, 63

Hui, C. Y., & Cheng, K. S. 2004, ApJ, 608, 935

Jahoda, K., Markwardt, C. B., Radeva, Y., et al. 2006, ApJS, 163, 401

Jahoda, K., Swank, J. H., Giles, A. B., et al. 1996, in Society of Photo-Optical Instrumentation Engineers (SPIE) Conference Series, 2808, eds. O. H. Siegmund, & M. A. Gummin, 59

Jones, D. H. P., Smith, F. G., & Nelson, J. E. 1980, Nature, 283, 50

Kanbach, G. 1990, in The Energetic Gamma-Ray Experiment Telescope (EGRET) Science Symposium, NASA Conference Publication, 3071, eds. C. E. Fichtel, S. D. Hunter, P. Sreekumar, & F. W. Stecker, 101

Kuiper, L., Hermsen, W., Cusumano, G., et al. 2001, A&A, 378, 918

Kuiper, L., Hermsen, W., Walter, R., & Foschini, L. 2003, A&A, 411, L31

Link, B., & Epstein, R. I. 1997, ApJ, 478, L91

Link, B., Epstein, R. I., & Baym, G. 1992, ApJ, 390, L21

Lyne, A. G., Pritchard, R. S., & Graham-Smith, F. 1993, MNRAS, 265, 1003

Melatos, A. 2000, MNRAS, 313, 217

Mineo, T., Ferrigno, C., Foschini, L., et al. 2006, A&A, 450, 617

Nolan, P. L., Arzoumanian, Z., Bertsch, D. L., et al. 1993, ApJ, 409, 697

Oosterbroek, T., Cognard, I., Golden, A., et al. 2008, A&A, 488, 271

Oosterbroek, T., de Bruijne, J. H. J., Martin, D., et al. 2006, A&A, 456, 283

Özel, M. E. 1989, in Timing Neutron Stars, eds. H. Ögelman & E. P. J. van den Heuvel, 357

Özel, M. E. 1991, Europhysics Letters, 14, 275

Paul, B., & The LAXPC Team 2009, in Astrophysics with All-Sky X-Ray Observations, Proceedings of the RIKEN Symposium, eds. N. Kawai, T. Mihara, M. Kohama, & M. Suzuki, 362

Pravdo, S. H., Angelini, L., & Harding, A. K. 1997, ApJ, 491, 808

Romani, R. W., Miller, A. J., Cabrera, B., Nam, S. W., & Martinis, J. M. 2001, ApJ, 563, 221

Rothschild, R. E., Blanco, P. R., Gruber, D. E., et al. 1998, ApJ, 496, 538

Rots, A. H., Jahoda, K., & Lyne, A. G. 2004, ApJ, 605, L129

Sekimoto, Y., Hirayama, M., Kamae, T., & Kawai, N. 1995, ApJ, 443, 271

Staelin, D. H., & Reifenstein, E. C., III 1968, Science, 162, 1481

Tang, A. P. S., & Cheng, K. S. 2001, ApJ, 549, 1039

Tompkins, W. F., Jones, B. B., Nolan, P. L., et al. 1997, ApJ, 487, 385

Ulmer, M. P., Lomatch, S., Matz, S. M., et al. 1994, ApJ, 432, 228

Wills, R. D., Bennett, K., Bignami, G. F., et al. 1982, Nature, 296, 723

Wong, T., Backer, D. C., & Lyne, A. G. 2001, ApJ, 548, 447